The Journal of Experimental Biology 207, 853-868
Published by The Company of Biologists 2004
doi:10.1242/jeb.00821

Swimming of larval zebrafish: ontogeny of body waves and implications for locomotory development

Ulrike K. Müller* and Johan L. van Leeuwen

Wageningen University, Experimental Zoology Group, Marijkeweg 40, 6709 PG Wageningen, The Netherlands

*Author for correspondence (e-mail: ulrike.muller@wur.nl)

Accepted 3 December 2003

Summary

Fish larvae, like most adult fish, undulate their bodies to propel themselves. A detailed kinematic study of the larval body wave is a prerequisite to formulate a set of functional requirements that the locomotor system must fulfil to generate the observed swimming kinematics. Lateral displacement and curvature profiles were obtained for zebrafish (*Danio rerio*) larvae at 2–21 days post-fertilisation for three swimming behaviours (cyclic swimming, slow starts and fast startle responses) using high-speed video. During cyclic swimming, fish larvae maintain tail beat frequencies of up to 100 Hz. The corresponding longitudinal strains, estimated from the peak curvatures of the midline, reach up to 0.19 in superficial tissue. The strain rate can reach 120 s^{-1}. The wave of curvature travels along the body at a near-constant rate. Posterior to the stiff head, body-length-specific curvature is high and rises gently along the entire trunk to a maximum value of 6. Burst-and-coast swimming generates similar peak curvatures to cyclic swimming, but curvature rises more steeply from head to tail. Fish larvae exhibit phase shifts of 57–63° between the wave of lateral displacement and the wave of curvature, resulting in a 1:1.2 ratio of body wave length to curvature wave length. During C-starts, muscle strain can reach 0.19 and superficial longitudinal strain rates approach 30 s^{-1}. Fish larvae do not initiate their escape response with a standing wave of curvature, although their C-starts approach a standing wave as the larvae grow older. The performance demands derived from swimming kinematics suggest that larval axial muscles have very short contraction cycles (10 ms), experience considerable strains (up to 0.2) and strain rates (up to 30 s^{-1} in white muscle fibres) yet are able to power swimming for several seconds.

Key words: kinematics, *Danio rerio*, zebrafish, body wave, swimming, larva, muscle performance.

Introduction

Most fish generate travelling waves along their body to propel themselves: undulatory swimming is employed by many adult fish and is the prevalent locomotory mode in fish larvae. The body wave is powered by the axial muscles. The shape and speed of the body wave can provide useful information about the performance envelope of the fish's swimming muscles (Hess and Videler, 1984), mainly strains and strain rates, which can be derived from the curvature of the body wave. Adult body waves are roughly one body length long and sinusoidal (Videler and Hess, 1984). Due to the increasing amplitude envelope of the body wave, curvature of the body axis peaks near, but not at, the points of maximum lateral displacement (mackerel – Katz and Shadwick, 1998). The corresponding strains can reach up to 0.31 in the red muscle furthest from the body axis (carp – Spierts and van Leeuwen, 1999). Similar strains occur when the fish performs S- or C-starts (carp – Spierts and van Leeuwen, 1999).

The body wave is the product of the interaction between the contraction wave and the water surrounding the fish (Blight, 1977). The body influences the wave by its shape and its material properties. The water exerts viscous and inertial forces on the moving body. During ontogeny, a fish's body size and shape change dramatically, as do its swimming movements and the hydrodynamics governing its propulsion. As it grows, the larva experiences a change in flow regime. Flow regime depends on the viscosity (μ) and density (ρ) of the fluid, the body length of the organism (L) and its swimming speed (U), and it is best described by the relative importance of inertial and viscous forces. This ratio of fluid dynamic forces corresponds to the dimensionless Reynolds number (Re):

$$Re = UL\rho/\mu \, . \quad (1)$$

Fish larvae hatch at a body size of a few millimetres, which puts them in a transitional flow regime (Table 1; Re=50–900); adult fish live in an inertial flow regime (Re>1000). The different regimes demand different swimming styles and morphologies (Weihs, 1980; Webb and Weihs, 1986). Accordingly, we expect to observe the following changes in the swimming kinematics, which are consistent with inertia and lift replacing viscous forces as the main propulsive forces.

Table 1. *Kinematic parameters for zebrafish larvae during cyclic swimming and slow starts*

Age (days)	L (mm)	$\overline{U}_1$ (s^{-1})	*sm*	f (s^{-1})	A	U/V	J	S	α_a (deg.)	λ	Re	N_{tb}
Cyclic swimming												
2	3.5	9.3±3.0 (25)	±1.8 (5)	40	0.22	0.28	0.26	0.23	49	0.96	100	5
2	3.5	37.5±6.1 (14)	±0.6 (2)	71	0.20	0.48	0.65	0.53	34	1.05	450	2
3	3.9	8.1±2.7 (32)	±1.0 (5)	31	0.26	0.27	0.26	0.27	49	1.01	100	5
3	3.9	55.3±7.9 (11)	±0.9 (3)	100	0.23	0.55	0.69	0.55	23	1.09	850	3
4	4.2	43.8±3.2 (15)	±0.2 (2)	68	0.24	0.56	0.68	0.64	27	1.03	750	2
5	4.3	16.0±1.4 (24)	±2.7 (2)	42	0.19	0.38	0.51	0.38	46	0.99	300	2
5	4.3	48.4±8.0 (12)	±0.9 (5)	80	0.25	0.51	0.61	0.60	30	1.02	900	5
7	4.4	17.8±0.9 (18)	±0.0 (2)	56	0.11	0.36	0.70	0.32	36	0.94	350	2
7	4.4	44.9±5.8 (14)	±0.0 (2)	73	0.21	0.53	0.72	0.62	26	1.15	900	2
Slow start (values for second tail beat)												
2	3.5	3.9±0.7 (16)	±2.7 (13)	61	0.14	0.03	0.07	0.04	65	0.70	50	13
4	4.2	4.1±1.0 (36)	±1.1 (7)	28	0.12	0.04	0.21	0.10	70	0.76	70	7
7	4.4	4.9±0.4 (30)	±1.5 (6)	33	0.11	0.06	0.24	0.11	68	0.86	100	6
14	6.4	7.0±0.7 (33)	±1.1 (5)	30	0.17	0.06	0.23	0.16	52	0.81	300	5

Each row contains the data for one sequence. For cyclic swimming, the slowest and the fastest sequence is given if it contains more than one tail beat.

L, body length; $\overline{U}_1$, specific mean swimming speed ± S.D. (N, number of frames); *sm*, S.D. of mean swimming speed (N, number of tail beats); f, tail beat frequency; A, tail beat amplitude; U/V, slip; J, advance ratio; S, stride length; α_a, angle of attack of the tail; λ, body wave length; Re, Reynolds number; N_{tb}, number of tail beats analysed.

(1) Undulatory thrust oscillates as the tail beats back and forth, and so does swimming speed. As inertial forces increase in importance and drag decreases during yolk sac absorption, oscillations in the instantaneous swimming speed should become less pronounced. (2) Drag-based propulsion requires the propulsive element to move faster backward than the body moves forward; lift-based propulsion knows no such limitation. If lift mechanisms take over from drag as the main propulsive forces, then swimming speed should increase relative to body wave speed. (3) Narrow amplitude envelopes are more efficient than wide ones at high Re. The amplitude envelope of the body wave should narrow in the anterior part of the body until mainly the tail section performs lateral oscillations. (4) Fish larvae have low absolute swimming speeds due to their small size. To reach sufficient speeds to escape large predators, they have to generate high length-specific swimming speeds. To this end, larvae need to generate extreme tail beat frequencies (Bainbridge, 1958; reported values for zebrafish are ≤100 Hz – Buss and Drapeau, 2001). Tail beat frequency should drop as absolute swimming speed increases with increased body length. Locomotory apparatus and control are still developing in larvae, introducing further constraints on locomotion. Neural control of the locomotory apparatus is not yet fully established (e.g. Triller, 1997). Muscle fibre arrangement and fibre type change during ontogeny (van Raamsdonk et al., 1978). Zebrafish larvae hatch with a notochord and develop a vertebral column several days after starting to swim. (5) These changes in the locomotory system might affect the bending behaviour of the body and the shape of the body wave. (6) The finfold is gradually replaced as paired and unpaired fins develop, which changes the distribution of propulsive surfaces. The yolk sac is absorbed within the first few days after hatching, which will affect the distribution of drag forces. The combined changes in the distribution of propulsive and drag forces might affect the body wave as well as the stability and control of the larva's trim.

Body wave characteristics and their consequences for the locomotory system have been studied extensively in adult fish for fast starts, continuous and intermittent undulatory swimming (e.g. Johnston et al., 1995; Videler and Hess, 1984; Spierts and van Leeuwen, 1999). In adult fish, quantifying the body wave provided key insights into how fish power undulatory swimming (Hess and Videler, 1984; van Leeuwen et al., 1990; Katz and Shadwick, 1998), until the combination of sonomicrometry and electromyography allowed scientists to measure muscle strain and activation directly (e.g. Hammond et al., 1998; Wakeling and Johnston, 1998). In larval fish, however, the combination of these techniques is not (yet) feasible, and a detailed kinematic analysis is still a prerequisite for inverse dynamics fluid-mechanics models that predict net bending moments and generated power.

We aim to provide a rigorous overview of body wave characteristics and kinematic changes during ontogenetic development of swimming behaviour in zebrafish larvae. This study is a first step to understand changes in swimming style in relation to a changing flow regime and to formulate a set of functional requirements that the locomotor system (in particular, the swimming muscles) must fulfil to generate the observed swimming kinematics.

Materials and methods

Zebrafish (*Danio rerio* Hamilton 1822) larvae were reared in the laboratory from wild-type parents at the optimal rearing

temperature of 28°C. The larvae were fed *Paramecium* (5 and 6 days post-fertilisation) and *Artemia* (from 7 days onwards). We used sibling larvae 2, 3, 4, 5, 7 and 14 days post-fertilisation as well as sibling juveniles 21 days post-fertilisation. From 2 to 14 days, larval body length increased from 3.4±0.1 mm (N=6) to 6.6±1.1 (N=6) mm. The juvenile fish were 9.5±1.0 mm (N=6) long.

To record swimming behaviour, 10–20 sibling larvae of a given age group were transferred to a Petri dish (inner diameter 54 mm, water temperature 27°C). Swimming was recorded with a high-speed video camera (Redlake MotionPro, San Diego, CA, USA; 1000 frames s^{-1}, 1280×512 pixels, exposure time 124 μs) through a dissection microscope (Zeiss, Sliedrecht, The Netherlands; magnification 0.6–1.6× on the camera chip). The long axis of the field of view was between 9 mm and 12 mm. Juvenile fish were put in a Petri dish (inner diameter 88 mm) and filmed using the same high-speed camera and a 105 mm Nikon lens (Nikon Micro 105 mm 2.8, f stop 5.6, with a 27.5 mm extension ring, magnification 0.4–0.6×).

We recorded 40–120 swimming sequences for each age group. All age groups commonly perform spontaneous slow starts, extended episodes of cyclic fast swimming, referred to as 'cyclic swimming' in the remainder of the text, and fast starts, the latter often in combination with a change of swimming direction. We also elicited fast startle responses by touching the larva with a hair. We analysed four sequences of the slow and fast start behaviour for each age group. Each analysed sequence consisted of at least one complete tail beat. All age groups also occasionally exhibit cyclic swimming, of which we analysed up to 13 (age 3 days) and at least four (age 14 days) sequences for each age group. For each behaviour at each age group, we analysed between 10 (cyclic swimming of 5-day-old larvae) and 25 (slow start swimming of 2-day-old larvae) complete tail beats. The variation is due to the higher stride length of the older fish, which remain in the field of view for fewer tail beats.

Between 18 and 25 points were indicated manually on the midline of the fish to digitise the midline using MatLab 6.0. These raw midlines were interpolated and smoothed in space and time using a cubic spline fit with a user-defined smoothing factor of 0.0005 (Woltring, 1986) to obtain 51 equidistant points (for a more detailed description of the interpolation, smoothing and smoothing-factor criteria, see Johnston et al., 1995). We then derived the mean path of motion by linear regression through the positions of the snout and the tail tip. All midline coordinates in the camera frame of reference were rotated so that the larva's mean path of motion was made equivalent to the x-axis of the fish-based coordinate system. From the rotated and interpolated midlines, we obtained the following kinematic parameters. From the path of the tail tip relative to the mean path of motion, we derived tail beat amplitude (A; maximum lateral excursion of the tail tip) and tail beat frequency (f; reciprocal of the time it takes the tail to complete one tail beat). We define a tail beat as the tail moving from the centre line to one lateral extreme, then to the opposite lateral extreme and returning to the centre line. We derived the instantaneous lateral speed (v) of the tail tip from the position of the tail tip. Angle of incidence (α_i) and angle of attack (α_a) of the tail were defined as the angle between the line fit through the last five points of the midline and the mean path of motion, and the path of the tail tip, respectively. Swimming speed and acceleration were derived at the location of minimum lateral excursion of the midline, the pivot point, which served as a first approximation of the centre of gravity of the fish. Instantaneous swimming speed (U) and acceleration (a) were calculated from the displacement of the pivot point between consecutive frames. Mean swimming speed ($\overline{U}_1$) was calculated as the average of U over one complete tail beat. The body wave of an undulatory swimmer is defined by the wave of lateral displacement of its midline. Instantaneous body wave speed (V) and body wave length (λ) were determined from the zero positions of the midlines (points at which the midline crosses the mean path of motion) and their displacement between consecutive frames. To obtain swimming speed ($\overline{U}$), body wave speed ($\overline{V}$), lateral speed ($\overline{v}$) of the tail tip, and body wave length (λ) for the entire sequence, we averaged the instantaneous values of several complete tail beats. We further determined stride length (S; distance covered during one tail beat), advance ratio (J; ratio of $\overline{U}$ to $\overline{v}$) and slip (U/V; ratio of $\overline{U}$ to $\overline{V}$). For turning behaviour, we determined the maximum instantaneous angular velocity of the head (φ_{max}) and the turning angle (Φ). Curvature (κ) and rate of curvature ($d\kappa/dt$) were derived from the midlines as described by Lipschutz (1969) and Johnston et al. (1995):

$$\kappa = [(d^2F/ds^2)^2 + (d^2G/ds^2)^2]^{0.5} / [(dF/ds)^2 + (dG/ds)^2] , \quad (2)$$

with the functions F and G describing the midline position in x and y as a function of position s along the body at time t: $x=F(s,t)$, $y=G(s,t)$. For more details, see Johnston et al. (1995). From the lateral displacement wave, or body wave, we also derived the wave of curvature, its wave length and wave speed. The computer programs to derive the smoothed midlines, instantaneous swimming speed and acceleration, curvature and rate of curvature were written in Fortran. All other kinematic parameters were derived from these data using command files written for MatLab 6.0 on a PC. Throughout the remainder of the text, all lengths are normalised by total body length (L); hence, lateral displacement (h), tail beat amplitude (A), body wave speed (V), swimming speeds (U, $\overline{U}_1$, $\overline{U}$), acceleration (a) and curvature (κ) are expressed as specific values, unless they are qualified as 'absolute' values.

To determine the errors of the digitising and filtering process, we digitised one sequence of each behaviour for age groups 2 days and 7 days five times. The standard errors of the mean tail beat amplitude, mean swimming speed and curvature are always less than 0.05. Position of maximum curvature has a standard error of <0.01.

Results

General swimming behaviour

Swimming behaviour was classified into three categories based on turning angle, swimming speed and body wave

shape. Cyclic swimming (Fig. 1A) was characterised by the following criteria: (1) a wide body wave amplitude along the entire body, (2) a near constant and high swimming speed ($\overline{U}_1$>7 s^{-1}) that was maintained for the entire time that the fish was in the field of view and (3) a straight mean path of motion. Slow starts (Fig. 1B) were characterised by (1) a narrow amplitude envelope, (2) a low mean (<10 s^{-1}) and quickly declining $\overline{U}_1$, (3) a straight mean path of motion and (4) pectoral fins beating during the entire swimming episode. Fast startle responses (Fig. 1C) showed (1) large body curvature, including a C- or U-shaped phase, (2) a rapidly increasing swimming speed and (3) turning angles in excess of 30°. Swimming was considered to be cyclic if mean swimming speed changed by less than 10% between consecutive tail beats. The criterion for a straight mean path of motion was considered violated if the larva's heading changed by more than 15° during the recorded sequence (Fuiman and Webb, 1988). All analysed slow and fast starts were initiated when the larva was sitting on the bottom of the Petri dish. The height of the water column was 8 mm, and the larvae usually climb very little after a slow start, leaving them within the proximity of the bottom and hence within the influence of ground effects. During cyclic swimming, the larvae maintain a position in the middle of the water column outside the region of wall effects. Although early larvae often roll onto their sides when resting on the bottom, we analysed only those sequences in which the larva was upright when initiating a start and did not roll onto one side while swimming.

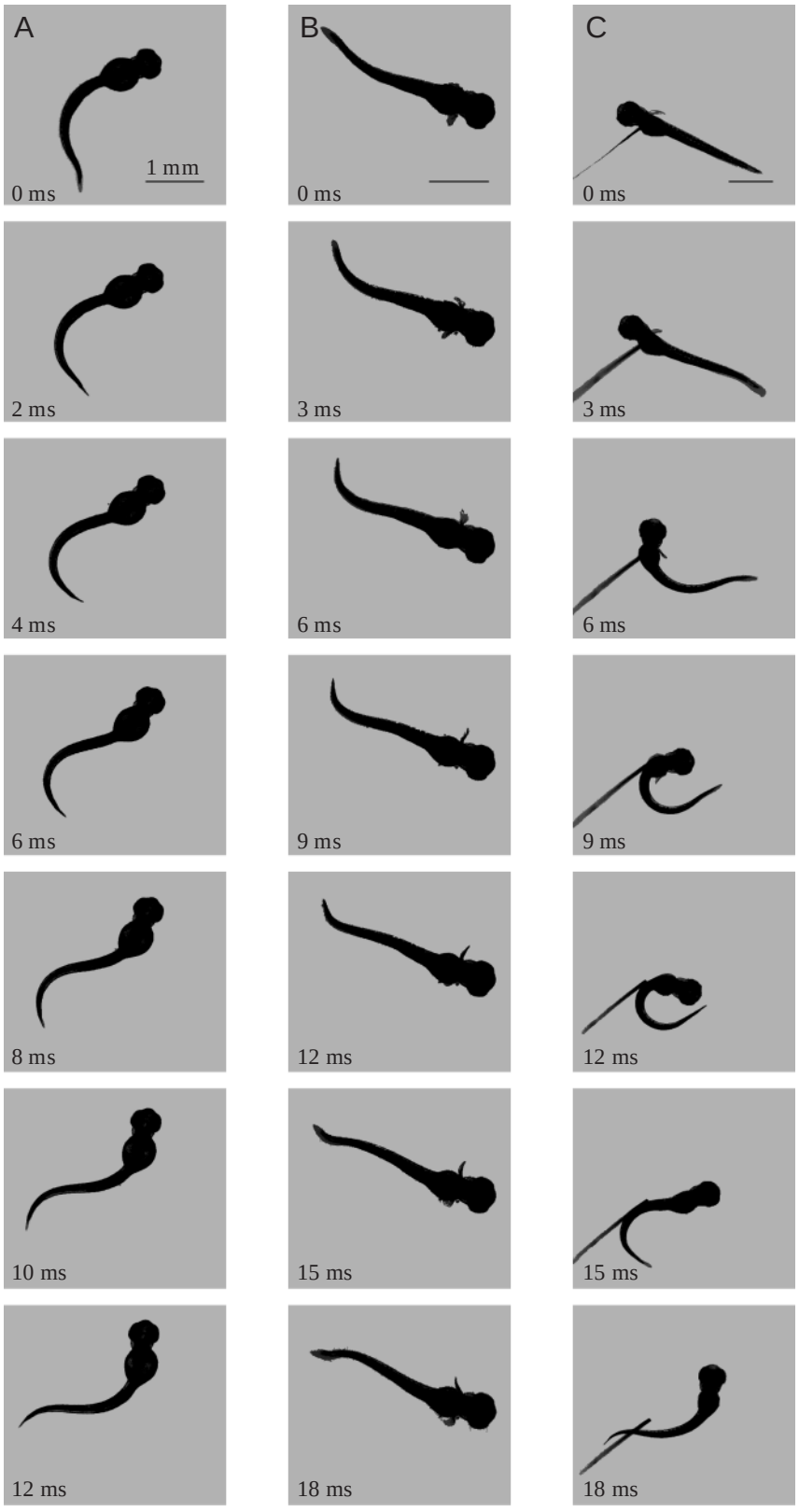

Fig. 1. Recordings of a swimming zebrafish larva for half a tail beat. (A) Cyclic swimming [age 3 days, mean swimming speed ($\overline{U}$)=8 s^{-1}]. (B) Slow start (age 2 days, $\overline{U}$=0 s^{-1}). (C) Fast turn (age 3 days). Scale bar, 1 mm.

Swimming activity increases with age: newly hatched zebrafish larvae spend most of their time resting on the bottom of the tank, while juveniles swim essentially all the time. Also, control increases substantially with age: the larvae maintain a dorso-ventral orientation in the water only gradually with increasing age, and swimming bouts of yolk-sac stages often commence while lying on their side. At age 2 days, larvae show substantial yaw and roll. They are occasionally unable to maintain directional stability and swim in tight circles or roll while swimming continuously. The proportion of cyclic swimming relative to burst-and-coast swimming decreases with increasing age. At age 2 days, 25% of all recorded spontaneous swimming behaviour

was classified as cyclic swimming. At age 4 days, this value had decreased to less than 5% of all recorded sequences. At age 5 days, cyclic swimming occurred rarely and only after strong startle stimuli (touching the larval tail with a hair).

Cyclic swimming

Zebrafish larvae, like juveniles, perform cyclic swimming episodes almost exclusively as part of a strong startle response, in which they maintain active swimming for more than 10 body lengths of travel instead of coasting after 3–5 tail beats. Across the entire age- and swimming-speed range of this study, cyclic swimming is characterised by a high swimming speed and a wide amplitude envelope compared with those of slow starts (Table 1; Fig. 2i). Larvae reach mean swimming speeds ($\overline{U}_1$) of 8–55 s^{-1}. The highest $\overline{U}_1$ of 55 s^{-1} was recorded for a 3-day-old larva swimming at a tail beat frequency of 100 Hz.

High tail beat frequencies lead to high lateral velocities of the tail compared with swimming speed (cf. path of the tail; Fig. 2ii, red lines). Coupled with the periodically high angles of incidence at the tail tip (Fig. 3), such low advance ratios indicate that unsteady hydrodynamic effects might affect the tail's performance as a propulsor. The tail also maintains a rather high angle of attack of 40–50° while traversing (Fig. 3). Instantaneous swimming speed (U) and lateral speed of the tail (v) both peak twice per tail beat at similar moments during the tail beat, suggesting that the tail contributes significantly to the propulsion.

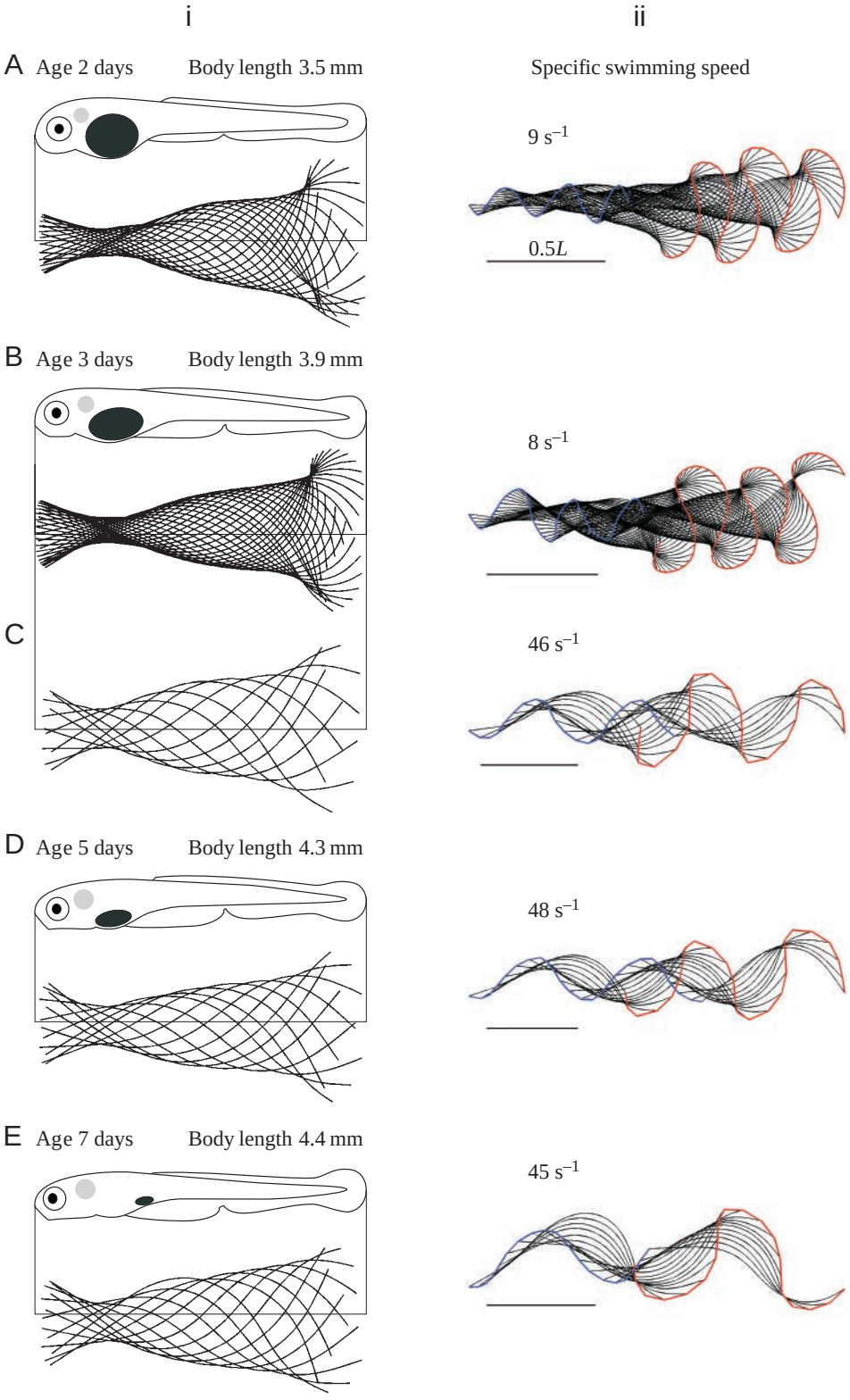

Fig. 2. Midline kinematics of zebrafish larvae (A–E; age 2, 3, 5 and 7 days post-fertilisation) during cyclic swimming. (i) Lateral view of the larva and midlines in a fish-based frame of reference. The superimposed midlines (time step 1 ms, scaled to the lateral view of the larva) of one tail beat cycle show the amplitude envelope of the body wave. The envelope has a minimum at 0.16–0.21 body length (L) located within the anterior third of the yolk sac (black oval: yolk sac; grey circle: otic placode at ~0.16L). All larvae are scaled to be the same length. (ii) All midlines (black) of the recorded sequence (time step 1 ms) in an earth-based frame of reference. The path of the head and the tail are indicated in blue and red, respectively. The scale bar indicates 0.5L. The sequences were chosen for a similar swimming speed for the two categories 'slow' and 'fast' swimming.

The oscillations in U depend on the $\overline{U}_1$ of the particular tail beat. At a low $\overline{U}_1$ of 8 s^{-1}, a 3-day-old larva reaches an *Re* of only 30. Compounded by a sizeable yolk sac, drag is high. The larva's inertia is too low to smooth out the periodic nature of its thrust generation and U changes by a factor of three during one tail beat. These oscillations decrease with increasing $\overline{U}_1$ and *Re* (Table 1).

To quantify the unique features of larval body waves and eventual changes with swimming speed and age, we calculated profiles for lateral displacement (h) and curvature (κ) (Fig. 4). A horizontal transect through the displacement profile at time t corresponds to the midline or body wave for this instant in time (Fig. 4A,C, red lines on contours and transect A1). During cyclic swimming, the larval body wave is roughly 1.0L long (Fig. 4A): the horizontal transect (red line) crosses or touches three h_0 contours (thick, black lines). Body wave length is not constant along the body: the distance between the 1st and 2nd zero transection is shorter than the one between the 2nd and 3rd.

For a travelling wave, an increase in wave length along the body is equivalent to an increase in wave speed. Wave speed can also be gleaned from the displacement profile by

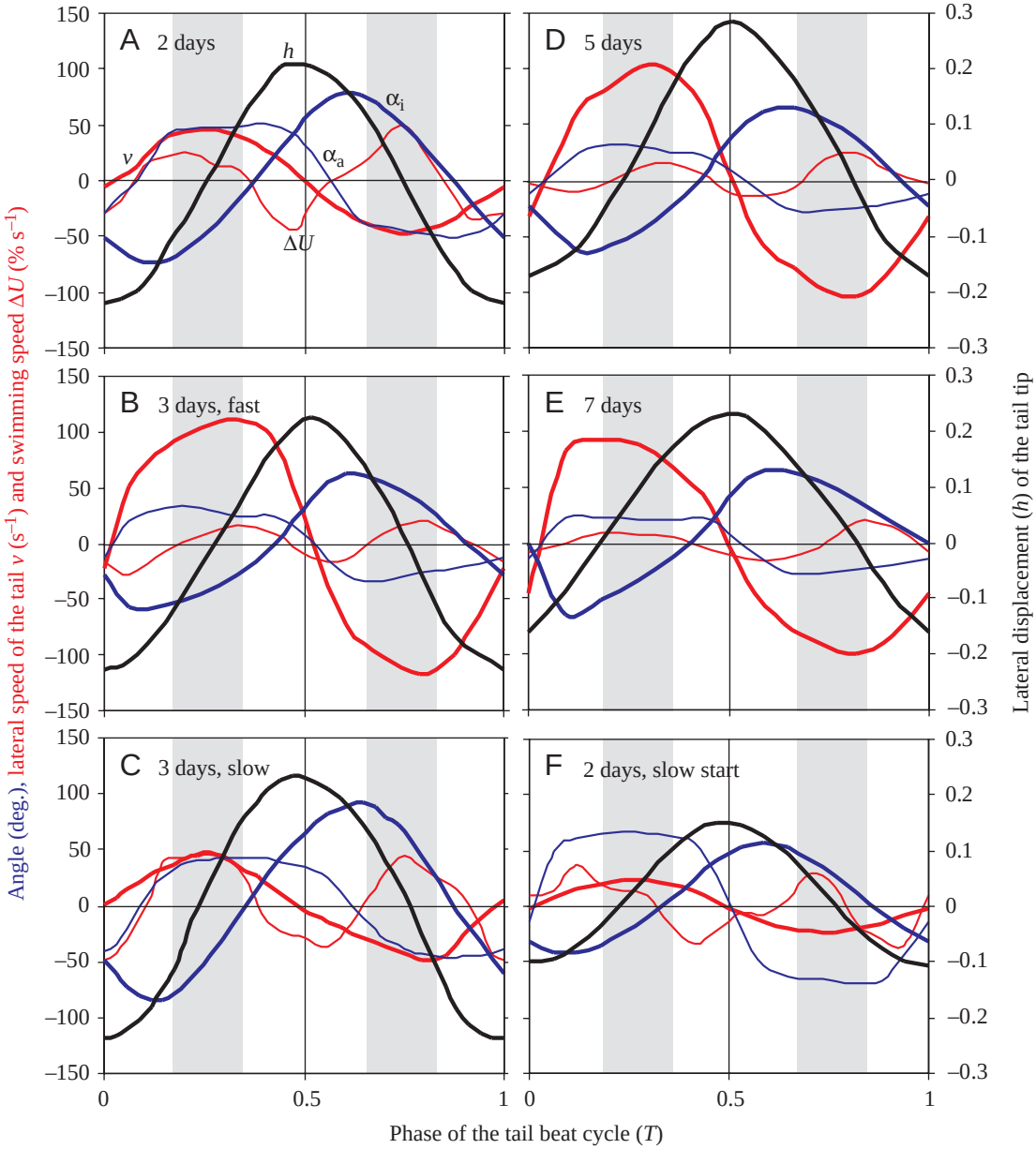

Fig. 3. Tail beat kinematics of zebrafish larvae (age 2, 3, 5 and 7 days post-fertilisation) during cyclic swimming and a slow start (age 2 days). Lateral position of tail tip (h; black), swimming speed (ΔU; thin red line), lateral speed of tail tip (v; thick red line), angle of incidence (α_i; thick blue line) and angle of attack (α_a; thin blue line) of the tail over one tail beat cycle. All values are means based on two (age 7 days) or three tail beat cycles of one swimming sequence. The grey bars indicate roughly when swimming speed reaches a maximum during the tail beat cycle. ΔU is expressed as % deviation from the specific swimming speed averaged over one complete tail beat ($\overline{U}$): $\Delta U=(U-\overline{U})/\overline{U}$.

establishing the shape of the h_0 contour (Fig. 4A, thick, black lines): a straight contour indicates that the body wave travels along the body at a constant speed. Because the stiff head of a fish cannot submit to the body wave, larval body waves change their speed along the body. At the snout, the h_0 contour starts off almost horizontal: the wave behaves almost like a standing wave (wave speed 63 s^{-1}, N=30, r^2=0.92). Behind the snout, the slope of the h_0 contour rises sharply, indicating that the body wave slows down (wave speed 17 s^{-1}, N=30, r^2=0.99). The slope drops again behind the head, and wave speed is nearly constant along the remainder of the body (wave speed 33 s^{-1}, N=200, r^2=0.92). Following the extremes (h_{max} contour: Fig. 4A,C contour and transect A1, broken black line) rather than the h_0 contour of the lateral displacement profile is equivalent to tracing the amplitude envelope. Between the pivot point and the tail, lateral displacement increases gradually along the h_{max} contour for the fast swimming sequence (Fig. 2C), which corresponds to the gradually widening amplitude envelope. During slow swimming (Figs 2B, 4A), the amplitude envelope widens first very gradually and then fans out quickly at the tail: the h_{max} contour traces a much steeper rise in lateral displacement at the tail compared with the fast-swimming sequence (Fig. 2C, 5B). A vertical transect through the displacement profile at a point s along the body shows the shape of the propulsive wave (Fig. 4A,C, cyan line).

The wave of curvature (Fig. 4B) is a function of the wave of lateral displacement (Fig. 4A). The difference in their respective amplitude and phase depends on the shape of the body wave (Katz and Shadwick, 1998). Due to the stiff head,

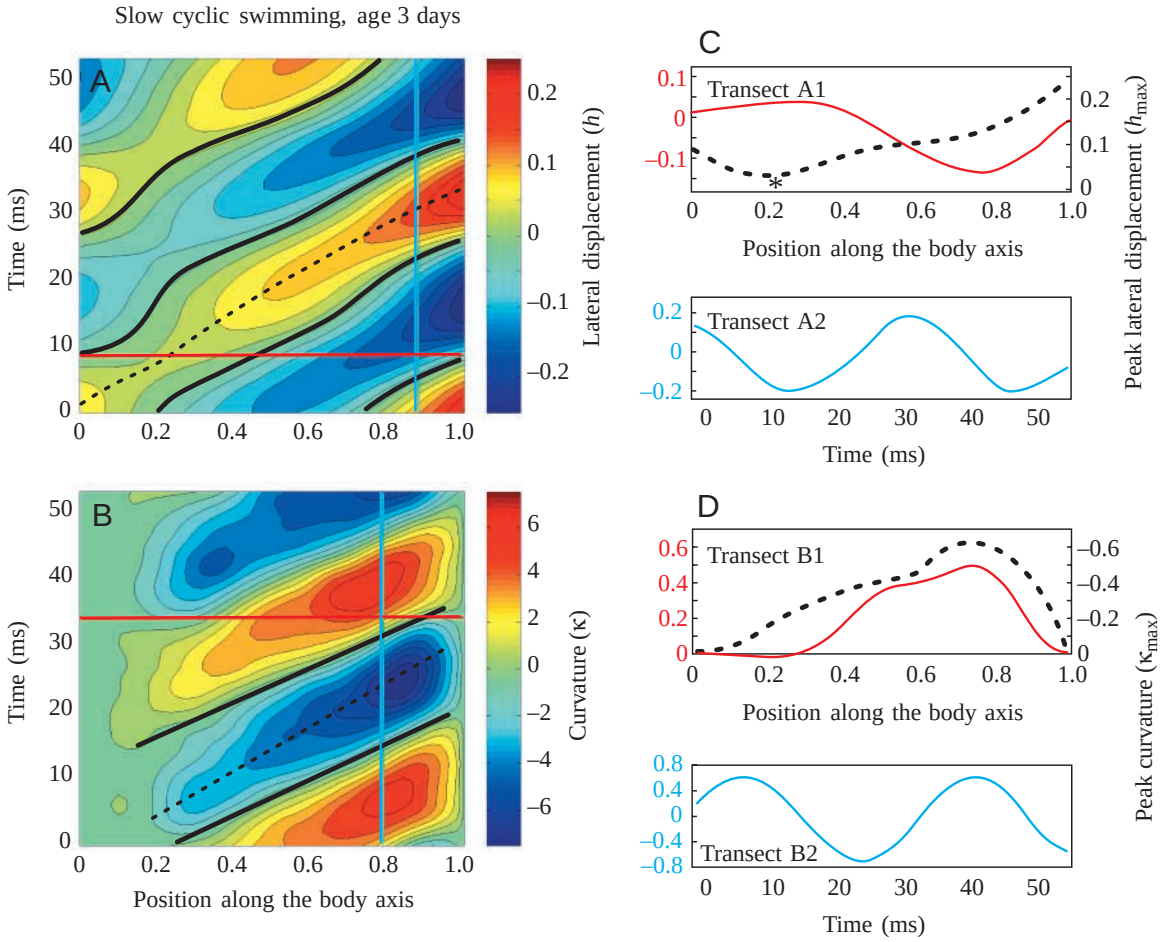

Fig. 4. Cyclic swimming in zebrafish larvae (3 days post-fertilisation; $\bar{U}$=8 s^{-1}) (A) Contours of the specific lateral displacement (negative values = displacements to the left of the larva) and (B) specific curvature (negative values = convex curvature), plotted along the body axis (x-axis) and in time (y-axis) for two complete tail beats. (C,D) Vertical and horizontal cross sections through the displacement (A) and the curvature contours (B), respectively. The contours correspond to Fig. 2B. The thick, black lines indicate zero lateral displacement (h_0) and zero curvature (κ_0) in A and B, respectively. The broken black lines indicate the changing position in time and space of local extremes in lateral displacement (h_{max}) and curvature (κ_{max}), which correspond to the amplitude envelope of the displacement (transect A1; the asterisk indicates pivot point) and the curvature wave (transect B1). Horizontal cross sections (red lines) indicate the body wave (A,C, transect A1) and curvature wave (B,D, transect B1), respectively. The distance between the points at which the horizontal cross section crosses the h_0 and κ_0 contours, respectively, is equivalent to half the wave length of the body wave and curvature wave, respectively. The vertical cyan lines (C,D, transects A2 and B2, respectively) indicate vertical cross sections. They indicate the propulsive wave in the displacement profile (transect A2) and the curvature wave in the curvature profile (transect B2).

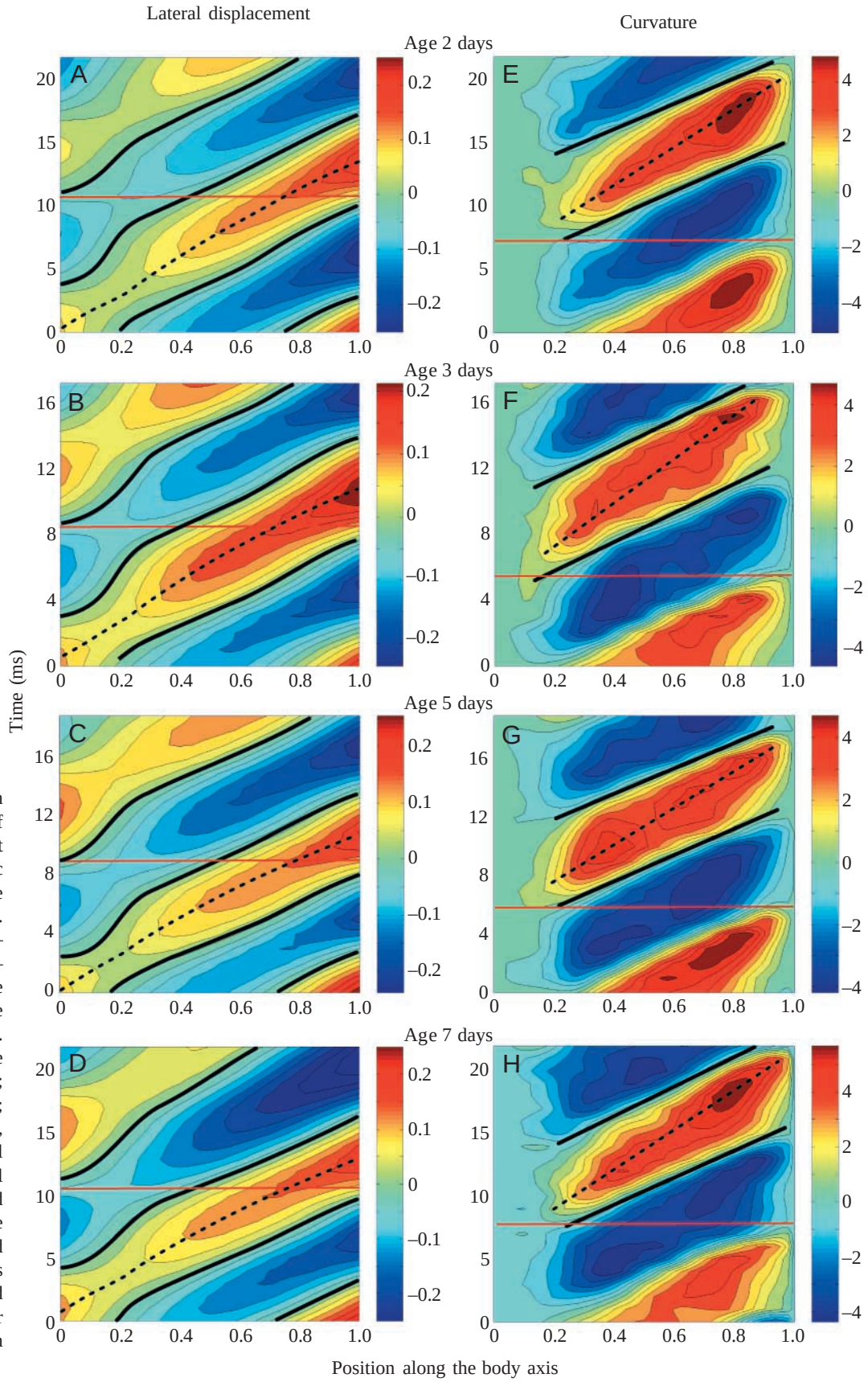

Fig. 5. Cyclic swimming in zebrafish larvae. Contours of the specific lateral displacement (left column) and specific curvature (right column) of the midlines of swimming larvae. Age post-fertilisation: A,E – 2 days; B,F – age 3 days; C,G – 5 days: D,H – 7 days. The contours are based on the same sequences as Fig. 2A,C,D,E. The thick, black lines indicate zero lateral displacement (h_0; A–D) and zero curvature (κ_0; E–H), respectively. Broken, black lines indicate the local extremes in the lateral displacement (h_{max}; A–D) and curvature (κ_{max}; E–H). The horizontal cross sections (red lines) indicate instantaneous body waves (A–D) and curvature waves (E–H). For further explanation, see main text and Fig. 4.

both waves are nearly instantaneous in the head region, then slow down along the head to continue at a constant speed along the remainder of the body. Yet they differ in their wave speed and wave length, as is born out by the difference in slope of the h_0 (Fig. 4A, thick, black line) *versus* the κ_0 (contour of zero curvature; Fig. 4B, thick, black line) contour. During slow swimming (Fig. 4), the slope of h_0 (corresponding wave speed 33 s^{-1}, N=200, r^2=0.99) is significantly steeper than that of κ_0 (corresponding wave speed 40 s^{-1}, N=200, r^2=0.98). This difference in slope introduces a phase shift between curvature and lateral displacement of 57° at the tail. During fast swimming, the phase shift is slightly higher (63°). This phase shift leads to the larval midline approaching a C shape during cyclic swimming; a horizontal line through the curvature profile barely transects more than one wave front and, at the highest swimming speeds, only transects one (Fig. 5E–H, red lines).

Horizontal and vertical transects through the curvature profiles also contain information about the body wave. The wave of curvature travels down the body at a nearly constant speed. Hence, the vertical transect though the curvature profile is an honest reflection of the local shape of the body wave without the distorting effects of the increasing amplitude envelope that affect the horizontal transect. Both transects reveal that the larval body wave is further removed from a pure sine wave than the body wave of an adult fish (e.g. Videler and Hess, 1984; Fig. 6). The curvature of the first quadrant of a pure sine wave increases at an increasing rate, whereas for a wave composed of semicircles, curvature remains constant between the step-like transitions from one semicircle to the next. The larval curvature profile lies between that of a pure sine and a semicircle: after a wide transition zone (corresponding to roughly 0.15λ), curvature approaches a plateau (corresponding to roughly 0.10λ).

The shape of the body wave depends on swimming speed. At high speeds (Fig. 5F *vs* Fig. 4B), the zones of extreme curvature are wider and the transition between extremes is steeper and narrower in both the vertical and the horizontal transects through the profile. Higher swimming speeds entail lower absolute curvatures (by up to 25%). At low swimming speeds, peak curvature during half a tail beat increases along the body: the ridge of the curvature profile rises steadily from the head to a maximum value near the tail (Fig. 4B, black broken line). During fast swimming, the ridge of the curvature profile (κ_{max}), rather than rising steadily along the trunk, can have several local maxima along the body at different moments during a half tail beat (Fig. 5G, black, broken line).

With increasing age, cyclic swimming episodes become increasingly rare. Absolute swimming speed increases with age, while specific swimming speed remains similar across the observed age range. Both strongly depend on tail beat frequency (Table 1; Fig. 7). With age, the oscillations in instantaneous swimming speed U within one tail beat decrease from a threefold difference between minimum and maximum values to less than a quarter at the low swimming speeds. But the oscillations remain considerable at the high swimming speeds, even at age 7 days (Table 1). Slip, the ratio of swimming speed to body wave speed, remains low across the studied age range and peaks at 0.56 at the highest swimming speeds (adult fish: 0.5–1.0; Videler, 1993).

Body wave length (0.8–1.2L) and tail beat amplitude (0.11–0.26L) vary considerably between swimming events (Table 1). But they change little with age and remain similar to values found in sperm cells, tadpoles and adult fish. The unique features of larval swimming (the fanning amplitude envelope and the high angles of incidence) disappear with increasing swimming speed and age. With increasing age, the body wave elongates less along the body (Fig. 5A–D, red

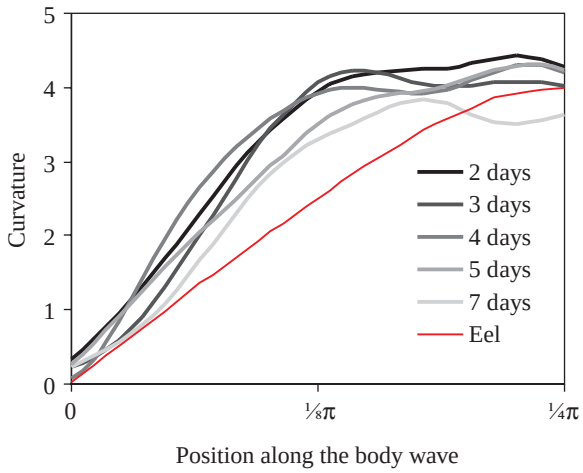

Fig. 6. Specific curvature along the first quadrant of the body wave in the posterior half of the body for zebrafish larvae (age 2–7 days post-fertilisation) during cyclic swimming (grey lines) and for juvenile eel (data re-analysed from Müller et al., 2000; red line) at the moment when the tail crosses the mean path of motion.

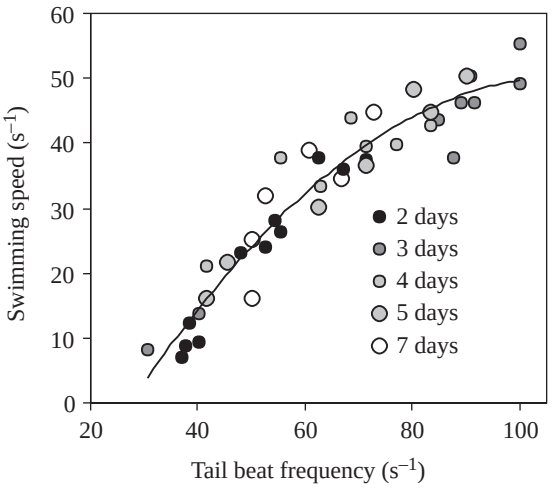

Fig. 7. Plot of specific swimming speed ($\overline{U}$) against tail beat frequency (f) for zebrafish larvae (age 2–7 days post-fertilisation) during cyclic swimming. The equation for the regression curve is f=–0.0076$\overline{U}^2$+1.65$\overline{U}$–39.58; r^2=0.92, total N=40.

lines). The larval curvature profile changes gradually towards a more sinusoidal profile (Fig. 6), but curvature remains high along the entire body for all cyclic-swimming sequences.

Slow start

Zebrafish of all ages exhibit burst-and-coast swimming. Newly hatched larvae often show no discernible displacement during these brief bursts (Fig. 1B) and are hypothesised to perform them not for locomotory but respiratory purposes (Osse and van den Boogaart, 1999): the body undulation and beating pectoral fins displace the surrounding water to replace it with fresh, oxygen-rich water. The still-developing pectoral fins of hatchlings generate a backward flow and do not counteract the body undulations to keep the body stationary (U. K. Müller and J. L. van Leeuwen, personal observation). Rather, the combined propulsive forces of fins and body are insufficient to overcome the larva's inertia and the adhesion to the bottom of the Petri dish. One day after hatching, at age 3 days, most weak bursts result in small displacements. Swimming speed peaks early during the burst, and peak speed increases from 0 for newly hatched larvae to up to 8 s^{-1} at age 14 days. Instantaneous swimming speed oscillates within one tail beat, although to a lesser degree than during cyclic swimming (Table 1), probably aided by the pectoral fins: pectoral fin beat matches the frequency, but not always the phase, of the tail beat, which can cause additional oscillations in the instantaneous swimming speed. Compared with cyclic swimming, body wave length is shorter (0.7–0.9*L*; Table 1) and increases little along the body. The amplitude envelope remains narrow along the body. It widens in the tail region but does not fan: the tail's angle of incidence is 15–20° lower during slow starts than during cyclic swimming. Despite the lower angle of incidence, angle of attack of the tail is higher than during cyclic swimming; as advance ratio approaches 0, angle of attack increases from values below 60° to values above 70°. However, the phase between angle of attack and lateral position and velocity of the tail are similar to cyclic swimming: the larva maintains similar tail beat kinematics and propulsive function of the tail during the slow starts (Fig. 3F).

The amplitude envelope of newly hatched larvae performing a slow start (Fig. 8i) is narrower than during cyclic swimming (Fig. 2i). The pivot point of the amplitude envelope is more posterior (0.25–0.31*L*) due to a different distribution of propulsive forces and their moments (Fig. 8i). First, the line of action of the body-generated propulsive force (and its lateral component responsible for the yaw) moves further posterior as the amplitude envelope narrows along the body. Second, the pectoral fins, which were adducted during cyclic swimming, beat during slow starts. This altered distribution of forces changes the position of the pivot point.

Tail beat amplitude nearly halves during one slow start sequence, with initial values similar to those of cyclic swimming. As soon as the larva begins to decelerate, tail beat amplitude drops, the entire amplitude envelope of the body wave narrows and slip increases. The amplitude envelope visibly contracts along the entire body over the duration of just one tail beat: the first midline of the tail beat (Fig. 8D, red midline) bends further outwards than the last midline (Fig. 8D, blue midline).

The lateral displacement and curvature profiles for slow starts (Fig. 8) differ from those for cyclic swimming (Figs 4, 5), but the extent of the difference strongly depends on swimming speed. Stronger starts (Fig. 8A,E) are initiated with a tail beat that resembles the cyclic-swimming kinematics (Figs 2C, 5F): the first tail beat shows a wide amplitude envelope and a high curvature along the entire body. Maximum instantaneous swimming speed (U_{max}) is reached at the end of the first tail beat and then quickly decreases as the larva adopts a more narrow amplitude envelope. Accordingly, curvature distribution changes considerably from the first to the last tail beat of a slow start. The curvature profile of the first tail beat consists of long diagonal zones of extreme curvature along most of the body (Fig. 8E, broken line). During the following tail beats (only one shown in Fig. 8E), the curvature extremes begin to concentrate more posteriorly in a fashion typical for slow starts (similar to curvature profiles in Fig. 8F,G, contours along broken line). Overall curvature decreases from one tail beat to the next, until the last tail beat barely registers on the curvature profile except for a weak peak at the tail. Maximum curvature occurs in the first or second tail beat and is similar to values during cyclic swimming.

Slow-start kinematics show similar age-related changes to those of cyclic swimming. Slip and advance ratio increase and tail beat frequency decreases. Terminal swimming speed and coasting distance increase. Amplitude envelope, curvature and wave shape do not change drastically with age. Tail beat frequencies are typically below 30 Hz but can reach 100 Hz during vigorous cyclic swimming in 3-day-old larvae. This means that swimming muscles of early fish larvae operate at frequencies of 30–100 Hz.

Fast startle response

Fish larvae often combine their brief swimming bursts with a change of swimming direction (Fuiman and Webb, 1988). We focused on startle responses away from the startle stimulus that were followed by several tail beats of swimming. Some startle responses were elicited by other larvae approaching or touching a larva; most were elicited by the experimenter touching or approaching the larva with a horse hair. All studied turns were initiated from rest when the larval body was straight and upright rather than rolled over to one side.

Newly hatched larvae (age 2 days) initiate a turn at the head: the head turns away from the stimulus, and a wave of curvature travels down the body at a speed similar to consecutive waves. The waves of bending and straightening the body associated with a C-start travel down the body at different speeds. Along the anterior two-thirds of the body (Fig. 9), the contours of the rising curvature gradient at the beginning of the C-start have a shallower angle with the horizontal of the contour plot than the contours of the falling curvature gradient – an angle of 0° with the horizontal corresponds to a standing wave. This suggests that the wave of bending travels faster than the wave

of straightening along most of the body. In young larvae, the bending wave starts at the head: the curvature contours start rising at the head, and the contour lines maintain a low angle with the horizontal until the last third of the body. At this point, the contour lines bend up and assume a much steeper angle: the wave of curvature slows down considerably. The wave of straightening the body travels from head to tail at a near constant speed: the falling curvature contours of the first half tail beat are not kinked like the rising contour lines but run straight along the entire body. The wave of straightening travels at a similar speed as the initial wave of bending along the anterior two-thirds of the body in young larvae. The profile of the first half tail beat differs from the profile of consecutive tail beats and cyclic swimming mainly in the higher curvature extremes reached during the first half tail beat. Startle responses show a more anterior maximum in curvature than episodes of cyclic swimming. Peak translational speed (determined at the pivot point at 0.22*L*) occurs as the body straightens after having adopted a C shape and coincides with maximum speed of the tail (Table 2). Peak translational acceleration (determined at the pivot point) precedes peak translational speed by roughly 1 ms (one frame of the recorded sequences). Maximum angular velocity of the head occurs earlier, when the body approaches a C shape. Peak translational accelerations reach 6×10^4 m s^{-2} (280 m s^{-2} or 28 ***g***; age 7 days), peak translational speeds reach 70 s^{-1} (0.3 m s^{-1}; age 4–7 days). Angular velocity of the head is approximately 26×10^3 deg. s^{-1} and decreases with age.

With increasing age, the speed of the initial wave of bending along the anterior body increases, while the speed along the

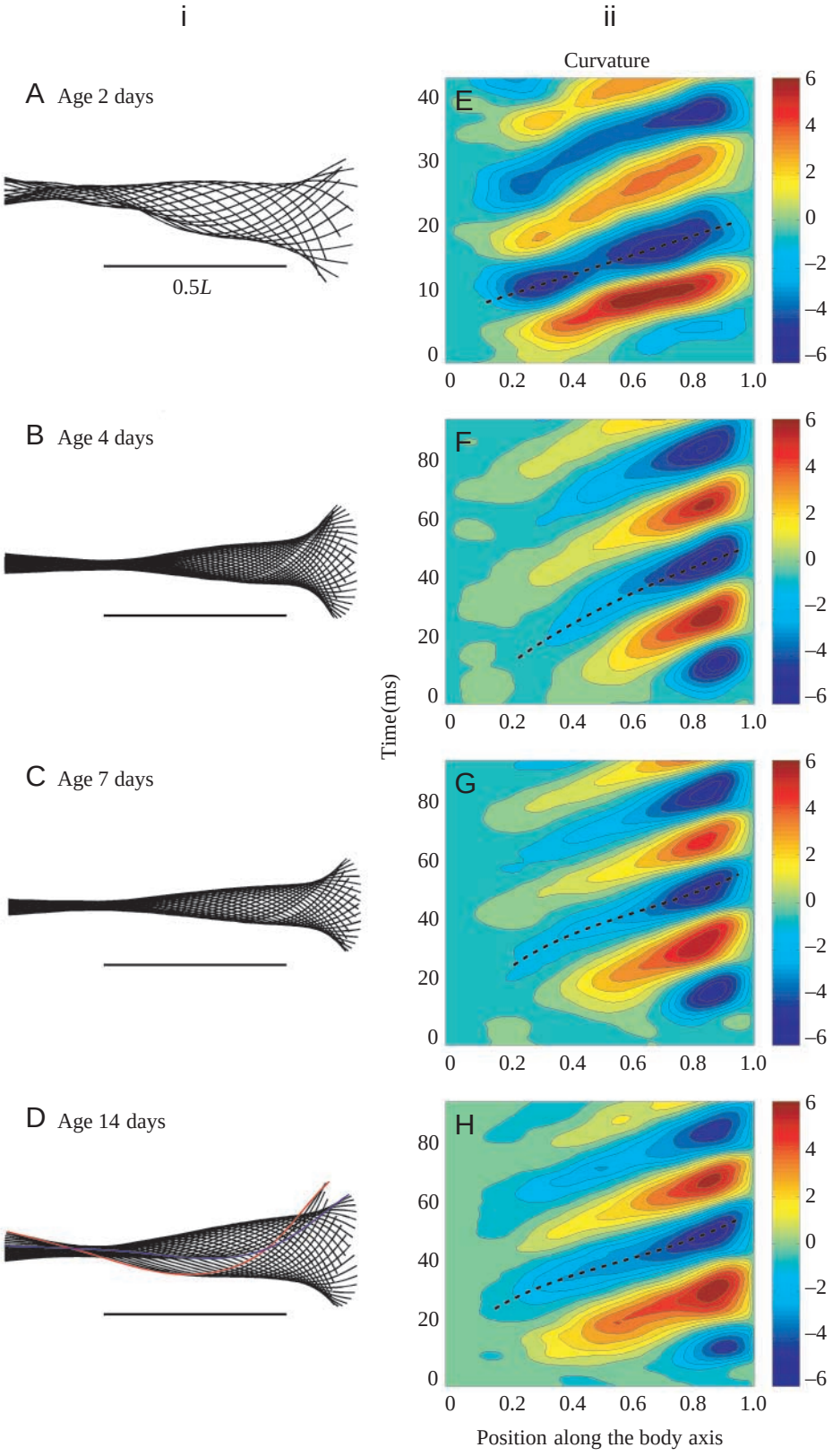

Fig. 8. Slow start of zebrafish larvae. Age post-fertilisation: (A) 2 days; (B) 4 days; (C) 7 days; (D) 14 days. (i) Amplitude envelope of the body wave. Larval midlines in a fish-based frame of reference for the 3rd tail beat cycle in the curvature profiles of the right column [time step 2 ms (A), 1 ms (B–D)]. Scale bar, 0.5*L*. In D, the 1st midline of the tail beat cycle is shown in red and the last midline in blue. (ii) Profiles of specific curvature. Contours of the specific curvature of the midlines, plotted along the body axis (*x*-axis) and in time (*y*-axis) for two complete tail beat cycles. The broken, black lines indicate the local curvature extremes.

posterior third of the body decreases. Consequently, the difference increases between the mean speed of the wave of bending and the speed of the wave of straightening. Also, the point around which the body starts to bend moves posteriorly. The zones of extreme curvature contract and become concentrated in the mid-body in 21-day-old fish. The total duration of the first half tail-beat becomes considerably longer than that of consecutive half tail beats. All this is consistent with the fish approaching the adult situation, in which the initial wave of bending occurs almost instantaneously and only becomes a travelling wave later during the C-start in the posterior section of the body (carp; Spierts and van Leeuwen, 1999). In adult C-starts, the wave of bending travels from head to tail at least twice as fast as the wave of straightening (carp; Spierts and van Leeuwen, 1999). The point around which the body bends initially (the first peak in curvature) lies roughly at 0.6*L* along the body axis in adult carp.

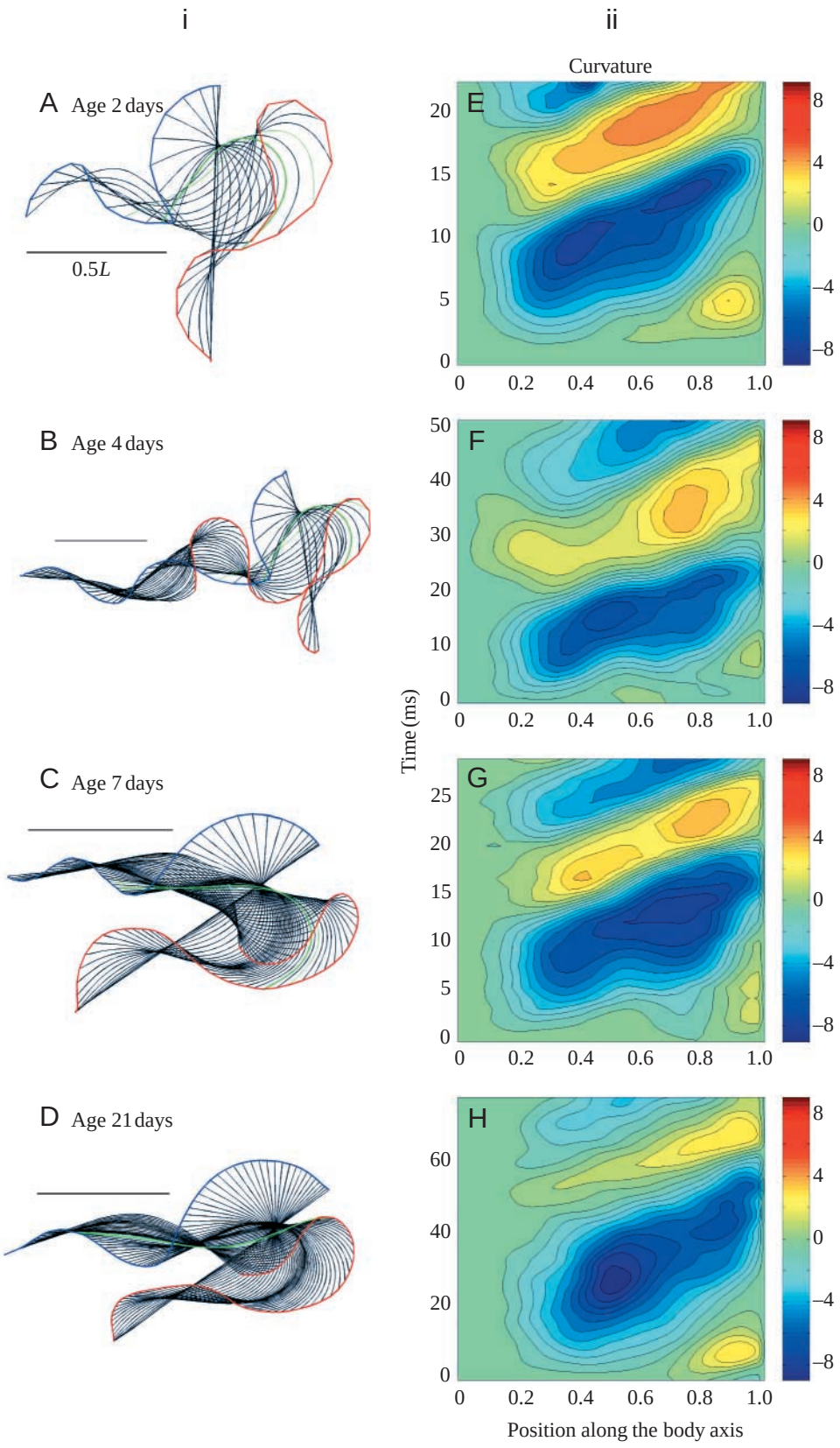

Fig. 9. Fast turn of zebrafish larvae. Age post-fertilisation: (A) 2 days; (B) 4 days; (C) 7 days; (D) 21 days. (i) Midlines of the larva in an earth frame of reference (time step 1 ms). Maximum translational speed: thin green midline; maximum acceleration: thick green midline. Scale bar, 0.5*L*. (ii) Profiles of specific curvature. Contours of the specific curvature of the midlines, plotted along the body axis (*x*-axis) and in time (*y*-axis) for one complete tail beat cycle.

Discussion

Developmental changes in the swimming kinematics

We predicted six trends in the swimming kinematics and body wave kinematics based on changes in the swimming hydrodynamics and morphology. First, with increasing age and body length, instantaneous swimming speed should oscillate less within one tail beat as inertial forces gain importance and the drag penalty of the shrinking yolk sac decreases. This trend is most clearly visible in the slow starts, for which we have data across a sufficient range of body lengths and ages (Table 1).

Table 2. *Kinematic parameters for zebrafish larvae during a fast turn*

Age (days)	U_{max} (s^{-1})	$t(U_{max})$ (ms)	a_{max} ($\times 10^3$ s^{-2})	$t(a_{max})$ (s)	φ_{max} ($\times 10^3$ deg. s^{-1})	$t(\varphi_{max})$ (ms)	Φ
2	54.35	14	38	12	26	7	95
2	67.38	17	38	16	28	7	95
3	64.58	16	24	15	23	7	50
4	72.46	14	29	11	25	6	76
5	69.93	16	49	15	20	5	81
7	69.61	20	63	19	26	5	153
14	20.27	36	17	34	12	10	146
21	22.71	58	8	57	7	16	126

U_{max}, maximum instantaneous swimming speed; $t(U_{max})$, time to reach U_{max}; a_{max}, maximum translational acceleration; $t(a_{max})$, time to reach a_{max}; φ_{max}, maximum angular velocity of the head; $t(\varphi_{max})$, time to reach φ_{max}; Φ, turning angle.

Cyclic swimming becomes increasingly rare and ceases to be performed spontaneously beyond age 4 days, when the larva is only 20% longer than at age 2 days. Second, the same limitations of the data are visible in the slip: only the slow-start data set is large enough to show the predicted trend (Table 1) across the studied age range. Slip increases not only with body length but also with swimming speed, which is consistent with the link between Reynolds number and propulsion mechanism that underlies the predicted relationship between slip and age. Third, the amplitude envelope of each of the three swimming behaviours does not change noticeably across the observed age range (Fig. 2). Rather, the behaviour associated with the wide amplitude envelope, namely the cyclic swimming, is replaced by burst-and-coast swimming with a narrower amplitude envelope (Fig. 8). Wakeling et al. (1999) observed an equivalent change in amplitude envelope towards the adult profile in carp larvae performing fast starts. Fourth, average tail beat frequencies for cyclic swimming do not change significantly (correlation coefficient=–0.1, N=65) over the observed age range. However, the frequency range drops from 30–100 Hz at age 3 days to 40–55 Hz at age 14 days.

Fish larvae (present study; carp – Osse and van den Boogaart, 1999), like sperm flagella (Brokaw, 1965; Lowe, 2003), approach a semicircular body wave. With increasing age, the larval body wave becomes more sinusoidal. Since a more semi-circular body wave does not seem to provide propulsive advantages in the more viscous flow regime, the reasons for the different wave shapes must be sought in developmental constraints imposed by the locomotor system (prediction 5; cf. Introduction). Changes in the bending behaviour can be due to changes in the structure and the material of the body and to changes in the muscles (and their control) that power bending. Adult fish possess a vertebral column consisting of stiff vertebrae linked by flexible joints; the notochord of ascidian and fish larvae is more homogeneously stiff. The notochord experiences a bending pattern with long stretches of barely changing curvature between short stretches of quickly changing curvatures (Fig. 10). Commensurate with a more homogenous bending stiffness, a more semicircular body wave avoids local peaks in the curvature, and we observe that absolute curvature is lower for the swimming sequences with more semicircular body

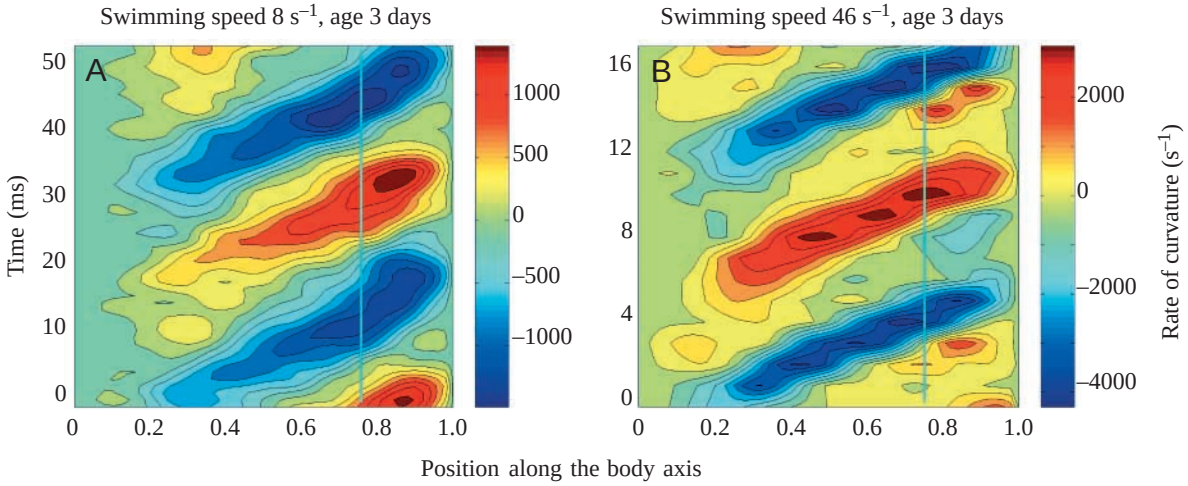

Fig. 10. Rate of curvature during cyclic swimming of zebrafish larvae. (A) Mean swimming speed over one complete tail beat ($\overline{U}$)=8 s^{-1} (corresponds to Figs 2B, 4). (B) $\overline{U}$=46 s^{-1} (corresponds to Figs 2C, 7B). The vertical profile for the higher swimming speed (B) exhibits wider plateaus with curvature rates near 0 and higher absolute extremes than that of slow swimming (A).

waves (Figs 4, 5) compared with more sinusoidal body waves (Fig. 8). On the other hand, the swimming muscles and their control might be unable to generate the contraction pattern necessary to generate a sine-shaped bending wave. A more semicircular body wave might help to avoid the high strain peaks associated with a sine body wave.

The larval body wave increases in length along the body. This is in contrast to several adult fish, whose body wave length remains approximately constant (eel – Müller et al., 2000; mackerel – Katz and Shadwick, 1998) or decreases posteriorly (pumpkinseed sunfish – McHenry et al., 1995). Wave length changes along the larval body, particularly at the transition from the head and yolk sac to the remainder of the body (Fig. 5A–D, red lines transecting thick, black lines). This local sudden change in wave speed might be associated with a change in the body's 2nd moment of area behind the yolk sac (prediction 6; see Introduction). However, even after the larva has absorbed most of its yolk at age 5 days, the body wave length still changes considerably along the body, unlike in adult fish, which maintain an almost constant wave speed (eel – data re-analysed after Müller et al., 2000; mackerel – Katz and Shadwick, 1998).

Yolk sac absorption, combined with the development of a swimbladder and pectoral fins, considerably improves the larva's trim (prediction 6; see Introduction). Hatchling larvae are not able to maintain a level body orientation and they nosedive as coasting speed approaches zero, whereas 4-day-old larvae keep a good trim while coasting.

During escape responses, both in fish larvae and adult fish, the wave of bending travels considerably faster along the body than the wave of straightening. In adult fish, the centre of bending is at 0.6*L* along the body (carp – Spierts and van Leeuwen, 1999). The adult wave of bending behaves initially like a standing wave (Spierts and van Leeuwen, 1999; Ellerby and Altringham, 2001) until maximum curvature is reached. This maximum begins to travel down the body at the speed that most authors report as the speed of the bending wave (e.g. Jayne and Lauder, 1993; Wakeling et al., 1999; Ellerby and Altringham, 2001). In early larval stadia, the initial bending wave is far from a standing wave and clearly travels down the body at a speed similar to that of consecutive waves (Fig. 9). The developmental changes in the turning behaviour towards a standing wave are most likely related to developmental processes rather than the transitional flow regime. The neural pathways that enable a simultaneous activation of all ipsilateral muscles are still developing, e.g. Mauthner axons are not yet myelinated at age 2 days (Triller et al., 1997).

In other respects, the swimming kinematics do exhibit changes that are consistent with a changing flow regime. During slow bursts, slip, stride length and advance ratio increase with body length and age.

Comparing kinematics of larval zebrafish with those of other undulatory swimmers

Detailed kinematic studies exist for adult fish, tadpoles, ascidian larvae and sperm flagella. Over this range of organisms, *Re* decreases by 10 orders of magnitude. Several chordate larvae swim in a similar flow regime to fish larvae at an *Re* of 10^1 (ascidian larvae) to 10^4 (large tadpoles). Sperm cells (Brokaw, 1965), ascidian larvae (McHenry, 2003) and tadpoles (Wassersug and von Seckendorf Hoff, 1985) have a similar amplitude envelope, while among adult fish only anguilliform swimmers such as the eel maintain a wide amplitude along the entire body (Gray, 1933). On first sight, adult eels use a similar swimming style to fish larvae. They not only exhibit a wide amplitude envelope but they also have a similar body shape and a finfold. Nevertheless, there are subtle differences in the shape of the body wave. Eels have a curvature profile that indicates a more sinusoidal body wave than the larval wave (Fig. 6). In zebrafish larvae, both body wave and curvature wave lengthen along the body from values near 1 to values around 1.2 and 1.5, respectively. By contrast, adult fish such as mackerel (Katz and Shadwick, 1998) and eel generate a wave of lateral displacement that travels at a constant speed; only their curvature wave accelerates along the body (data re-analysed from Müller et al., 2000). The difference in speed between the two waves causes an increasing phase shift along the body both in larvae as well as in adult fish. In adult mackerel, the phase shift between the lateral displacement wave and the wave of curvature reaches 54° at the tail. The larval amplitude envelope generates a slightly larger phase shift of up to 63°, which corresponds to a curvature wave that is ~20% longer than the body wave. This observation re-emphasises that lateral displacement is a poor indicator of curvature and muscle strain (Katz and Shadwick, 1998). First, for any amplitude envelope that is not either constant or increasing exponentially, a phase shift will occur between the lateral displacement function and body curvature. Second, white muscle fibres do not run parallel with the body axis, but their helical arrangement causes them to change orientation several times along the entire body (Gemballa and Vogel, 2002). This complex muscle architecture introduces further phase shifts (Shadwick et al., 1999). Without exact knowledge of the local fibre orientations and internal deformations, muscle strains cannot be deduced reliably from local curvature. Nevertheless, swimming kinematics does help to establish a performance envelope for swimming muscles by providing extreme estimates.

Swimming kinematics and muscle control

Our findings based on kinematics suggest that larval undulatory swimming puts severe demands on the axial muscles. Curvature of the body axis, combined with data on the local width of the body, can be used to estimate maximum longitudinal strains. In a 3-day-old zebrafish larva, curvature is high along the entire body during cyclic swimming: at 0.4 and 0.75 body lengths from the snout, curvature reaches 6.3 and 5.7, respectively. With a body width of 0.16 mm (at 0.75*L*) and 0.18 mm (at 0.4*L*), we obtain maximum longitudinal strains of 0.09 and 0.19, respectively, which would be experienced by the superficial red muscle fibres that run parallel with the body axis. During a startle response of a 3-day-old larva, strains in

the most superficial muscle layer reach 0.13 (0.19) at 0.75 (0.4)*L*. Larval strains are lower than in adult fish performing a C-start (0.17–0.28 during a C-start for carp; Spierts and van Leeuwen, 1999) but they are high compared with adult sprints (<0.1 for trout; Ellerby and Altringham, 2001). However, larval red muscles are unlikely to power these activities. Larval white muscle is located closer to the body axis, and white muscle fibres run at an angle with the body axis. Compared with the superficial tissue, longitudinal strains halfway between the body axis and skin are halved. Helical fibre orientation further reduces strains to values probably above 0.03 and closer to 0.05.

Such strains are high compared with other vertebrate muscles operating at cycle frequencies of 100 Hz (0.01 in sonic muscle of toadfish operating at 100 Hz; Young and Rome, 2001). The strain rates for larval swimming muscle can be estimated by differentiating the strain data in time. For cyclic swimming, this yields maximum strain rates of 70 (120) s^{-1} at 0.75 (0.4) body lengths from the snout using the superficial extreme strains of 0.09 and 0.19. Using the lower strain estimates (0.05) for white muscle fibres still yields strain rates of up to 30 s^{-1}, which is comparable with other fast locomotory muscles (Askew and Marsh, 2001).

We recorded five sequences in which fish larvae swam at speeds of up to 55 s^{-1} and tail beat frequencies of 90–100 Hz. Similar swimming speeds (up to 60 s^{-1} at 30°C; Fuiman, 1986) and tail beat frequencies (up to 70 Hz at 25°C – Budick and O'Malley, 2000; up to 100 Hz at 28.5°C – Buss and Drapeau, 2001) are reported in the literature. Muscle contraction cycle time is 10 ms at the highest tail beat frequency of 100 Hz, which is comparable to the fastest vertebrate muscles on record (swimbladder muscle of toadfish, 10 ms; Rome and Lindstedt, 1998). An important difference to the current record holders is that the larval swimming muscles must generate enough force to power swimming. High speed combined with high force production contradicts the hypothesis of the mutually exclusive muscle design stating that "*100 Hz is a feat impossible in locomotory muscle*" (Rome and Lindstedt, 1998; Young and Rome, 2001). This contradiction might be partly explained by scaling of muscle force with body size and can only be resolved once we know the power required for larval swimming. Larval locomotory muscles power "*sustained bursts of contractions ('burst swimming') at an average frequency of 60 to 70 Hz that last from several seconds to a minute duration*" (Buss and Drapeau, 2001). However, *in vitro* experiments on white muscle fibres on zebrafish embryos show tetanic fusion at stimulation frequencies above 30 Hz (Buss and Drapeau, 2001).

Larval swimming muscles are extreme performers: they operate at high strains and extreme strain rates. Yet, they still manage to generate enough force to propel the larva for a long period of time in an intermediate flow regime with considerable drag acting on the larva (for a review of typical performance envelopes of vertebrate muscles, see Woledge et al., 1985). We expect larval swimming muscles to share some of the special adaptations found in fast synchronous muscles; e.g. a considerable amount of sarcoplasmic reticulum to achieve the necessary Ca^{2+} rapid transport, high myosin ATPase rate and thin myofibrils. The non-sinusoidal body wave, particularly at the high swimming speeds, helps the larva to keep peak strains low but it does impose high strain rates (Fig. 10). The extreme strain rates strongly suggest that the fish larvae supplement their extreme muscle performance with elastic mechanisms to power cyclic swimming. Fish larvae only generate these very high tail beat frequencies during the first few days after hatching: maximum tail beat frequency drops with age. We therefore expect only young zebrafish larvae to possess these high-performance adaptations. Consequently, muscle protein isoforms should change rapidly during the first few weeks of larval development in response to the decreasing tail beat frequencies.

List of symbols

a	acceleration
A	specific tail beat amplitude
f	tail beat frequency (s^{-1})
F	function describing the x-position of the fish's midline in space and time
G	function describing the y-position of the fish's midline in space and time
h	specific lateral displacement of a particular point along the midline, $h=h(s,t)$
h_0	zero specific lateral displacement of the midline
h_{max}	maximum specific lateral displacement of the midline
J	advance ratio
L	body length (m)
Re	Reynolds number
s	specific position along the body ($0 \leq s \leq 1$)
S	specific stride length
t	time (s)
T	normalised phase of the tail beat ($0 \leq T \leq 1$)
U	specific instantaneous swimming speed (s^{-1})
$\overline{U}$	specific swimming speed, averaged over several complete tail beats (s^{-1})
$\overline{U}_1$	specific swimming speed, average of instantaneous swimming speed over one complete tail beat (s^{-1})
U/V	slip
U_{max}	maximum instantaneous swimming speed
ΔU	specific instantaneous swimming speed, normalised by $\overline{U}$ (% s^{-1})
V	specific instantaneous body wave speed (s^{-1})
v	specific instantaneous lateral velocity of the tail tip (s^{-1})
$\overline{v}$	specific lateral velocity of the tail tip, averaged over several complete tail beats (s^{-1})
$\overline{V}$	specific speed of the body wave, averaged over several complete tail beats (s^{-1})
x, y	Carthesian coordinate based in a fish frame of reference
Φ	turning angle (deg.)

α_a angle of attack of the tail (deg.)
α_i angle of incidence of the tail (deg.)
φ_{max} maximum angular velocity of the head (deg. s^{-1})
κ specific curvature of the midline, $\kappa=\kappa(s,t)$
κ_0 zero specific curvature of the midline
λ specific instantaneous body wave length
λ specific body wave length, averaged over several complete tail beats
ρ density
μ dynamic viscosity

We would like to thank Truus Wiegers and Talitha van der Meulen for providing fish larvae, and Jos van den Boogaart and Henk Schipper for help with the set-up. Sander Kranenbarg, Igor Spierts and two anonymous referees provided helpful comments on the manuscript. Jan Brascamp performed the error analysis of the digitising process. Funding to U.K.M. was provided by a visiting scientist scholarship from WIAS. All experiments were approved by the local ethics committee.

References

Askew, G. N. and Marsh, R. L. (2001). The mechanical power output of the pectoralis muscle of blue-breasted quail (*Coturnix chinensis*): the *in vivo* length cycle and its implications for muscle performance. *J. Exp. Biol.* **204**, 3587-3600.

Bainbridge, R. (1958). The speed of swimming of fish as related to size and to the frequency and amplitude of the tail beat. *J. Exp. Biol.* **35**, 109-133.

Blight, A. R. (1977). The muscular control of vertebrate swimming movements. *Biol. Rev.* **52**, 181-218.

Brokaw, C. J. (1965). Non-sinusoidal bending waves of sperm flagella. *J. Exp. Biol.* **43**, 155-169.

Budick, S. A. and O'Malley, D. M. (2000). Locomotor repertoire of larval zebrafish: swimming, turning and prey capture. *J. Exp. Biol.* **203**, 2565-2579.

Buss, R. R. and Drapeau, P. (2001). Synaptic drive to motoneurons during fictive swimming in developing zebrafish. *J. Neurophysiol.* **86**, 197-210.

Ellerby, D. J. and Altringham, J. D. (2001). Spatial variation in fast muscle function of the rainbow trout *Oncorhynchus mykiss* during fast-starts and sprinting. *J. Exp. Biol.* **204**, 2239-2250.

Fuiman, L. A. (1986). Burst swimming performance of larval zebra danios and the effects of diel temperature fluctuations. *Trans. Am. Fish. Soc.* **115**, 143-148.

Fuiman, L. A. and Webb, P. W. (1988). Ontogeny of routine swimming activity and performance in zebra danios (Teleostei: Cyprinidae). *Anim. Behav.* **36**, 250-261.

Jayne, B. C. and Lauder, G. V. (1993). Red and white muscle activity and kinematics of the escape response of the blue-gill sunfish during swimming activity. *J. Comp. Physiol. A* **173**, 495-508.

Gemballa, S. and Vogel, F. (2002). Spatial arrangement of white muscle fibres and myoseptal tendons in fishes. *Comp. Biochem. Physiol. A* **133**, 1013-1037.

Gray, J. (1933). Studies of animal locomotion. I. The movement of fish with special reference to the eel. *J. Exp. Biol.* **10**, 88-104.

Hammond L., Altringham, J. D. and Wardle, C. S. (1998). Myotomal slow muscle function of rainbow trout Oncorhynchus mykiss during steady swimming. *J. Exp. Biol.* **201**, 1659-1671.

Hess, F. and Videler, J. J. (1984). Fast continuous swimming of saithe (*Pollachius virens*): a dynamic analysis of bending moments and muscle power. *J. Exp. Biol.* **109**, 229-251.

Johnston, I. A., van Leeuwen, J. L., Davies, M. L. F. and Beddow, T. (1995). How fish power predatory fast-starts. *J. Exp. Biol.* **198**, 1851-1861.

Katz, S. L. and Shadwick, R. E. (1998). Curvature of swimming fish midlines as an index of muscle strain suggests swimming muscle produces net positive work. *J. Theor. Biol.* **198**, 243-256.

Lipschutz, M. M. (1969). *Theory and Problems of Differential Geometry*. *Schaum's Outline Series.* New York: McGraw-Hill.

Lowe, C. P. (2003). Dynamics of filaments: modelling the dynamics of driven microfilaments. *Proc. R. Soc. Lond. B* **358**, 1543-1550.

McHenry, M. J., Pell, C. A. and Long, J. H. (1995). Mechanical control of swimming speed: stiffness and axial wave form in undulatory fish models. *J. Exp. Biol.* **198**, 2293-2305.

McHenry, M. J. (2003). Mechanisms of helical swimming: asymmetries in the morphology, movement and mechanics of larvae of ascidian *Distaplia occidentalis*. *J. Exp. Biol.* **204**, 2959-2973.

Müller, U. K., Smit, J., Stamhuis, E. J. and Videler, J. J. (2000). How the body contributes to the wake in undulatory fish swimming: flow fields of a swimming eel (*Anguilla anguilla*). *J. Exp. Biol.* **204**, 2751-2762.

Osse, J. W. M. and van den Boogaart, J. G. M. (1999). Dynamic morphology of fish larvae, structural implications of friction forces in swimming, feeding and ventilation. *J. Fish Biol.* **55**, 156-174.

Rome, L. C. and Lindstedt, S. L. (1998). The quest for speed: muscles built for high-frequency contractions. *News Physiol. Sci.* **13**, 261-268.

Shadwick, R. E., Katz, S. L., Korsmeyer, K. E., Knower, T. and Covell, J. W. (1999). Muscle dynamics in skipjack tuna: timing of red muscle shorting in relation to activation and body curvature during steady swimming. *J. Exp. Biol.* **202**, 2139-2150.

Spierts, I. L. Y. and van Leeuwen, J. L. (1999). Kinematics and muscle dynamics of C- and S-starts of carp (*Cyprinus carpio* L.). *J. Exp. Biol.* **202**, 393-406.

Triller, A., Rostaing, P., Korn, H. and Legendre, P. (1997). Morphofunctional evidence for mature synaptic contacts on the Mauthner cell of 52-hour-old zebrafish larvae. *Neuroscience* **80**, 133-145.

van Leeuwen, J. L., Lankheet, M. J. M., Akster, H. A. and Osse, J. W. M. (1990). Function of red axial muscles of carp (*Cyprinus carpio* L.) recruitment and normalised power output during swimming in different modes. *J. Zool. Lond.* **220**, 123-145.

van Raamsdonk, W., Pool, C. W. and te Kronnie, G. (1978). Differentiation of muscle fiber types in the teleost *Brachydanio rerio*. *Anat. Embryol*. **153**, 137-155.

Videler, J. J. (1993). *Fish Swimming*. London: Chapman and Hall.

Videler, J. J. and Hess, F. (1984). Fast continuous swimming of two pelagic predators, saithe (*Pollachius virens*) and mackerel (*Scomber scombrus*): a kinematic analysis. *J. Exp. Biol.* **109**, 209-228.

Wakeling, J. M. and Johnston, I. A. (1998). Muscle power output limits fast-start performance in fish. *J. Exp. Biol.* **201**, 1505-1526.

Wakeling, J. M., Kemp, K. M. and Johnston, I. A. (1999). The biomechanics of fast-starts during ontogeny in the common carp *Cyprinus carpio*. *J. Exp. Biol.* **202**, 3057-3067.

Wassersug, R. J. and von Seckendorf Hoff, K. (1985). The kinematics of swimming in anuran larvae. *J. Exp. Biol.* **119**, 1-30.

Weihs, D. (1980). Energetic significance of changes in swimming modes during growth in larval anchovy, *Engraulis mordax*. *Fish. Bull.* **77**, 597-604.

Webb, P. W. and Weihs, D. (1986). Functional locomotor morphology of early life history stages of fishes. *Trans. Am. Fish. Soc.* **115**, 115-127.

Woledge, R. C., Curtin, N. A. and Homsher, E. (1985). *Energetic of Aspects of Muscle Contraction*. London: Academic Press.

Woltring, H. J. (1986). A Fortran package for generalised, cross-validatory spline smoothing and differentiation. *Adv. Eng. Software* **8**, 104-113.

Young, I. S. and Rome, L. S. (2001). Mutually exclusive muscle designs: the power output of locomotory and sonic muscles of the oyster toadfish (*Opsanus tau*). *Proc. R. Soc. Lond. B* **268**, 1965-1970.